The 2009 IEEE/RSJ International Conference on
Intelligent Robots and Systems
October 11-15, 2009 St. Louis, USA

Development of Spherical Ultrasonic Motor as a Camera Actuator for Pipe Inspection Robot

Masahiko Hoshina, IEEE *Student member*, Tomoaki Mashimo, IEEE *member*, and Shigeki Toyama

***Abstract*—We present a pipe inspection robot using a newly developed spherical ultrasonic motor (SUSM) as a camera actuator. The novel SUSM has improved the range of movement compared to previous SUSMs, and the robot can point a camera in any direction. In this study, we determined a method for controlling the rotational direction and strategic control from the kinematics and characteristics of ultrasonic motors. The rotational directions were defined by the phase differences of the applied voltages, and the rotational speeds were changed with the frequencies. Additionally, we developed a very small position sensing system using rotary potentiometers. In the control experiment performed using the sensing system, the SUSM showed the returnability to the default position from several specified points, within an accuracy of 1°.**

I. Introduction

VERY large scale gas and water pipe infrastructure exists under the ground and in buildings. In Japan, the overall length of this infrastructure is twelve billion kilometers. Many years have passed since its construction, and hence, inspections are necessary for ensuring safety. Atomic power plants, in particular, require new inspections to ensure safety from occasional potentially severe accidents. Although pipe inspection robots have been used for the inspection of small-diameter pipes, no robots having camera actuators with three rotational degrees of freedom (DOFs) exist for pipes with diameters less than 100 mm, due to the space constraint.

Many research groups have attempted the development of compact pipe inspection robots with new actuation to detect flaws and rust in pipe directories [1]–[10]. Pipe inspection devices using a camera with fish-eye lens suffer from the disadvantage that small details cannot be observed. Pneumatic actuators [1–3], shaped memory alloys (SMAs) [4], piezoelectric actuators [5, 6], and giant magnetostrictive alloys [7] have been employed to incline the head carrying the camera in the robots. Pneumatic wobble motors, which are compact and flexible actuators, rotate the camera and hands of the robot [8]. Snake robots, which aim to move in a pipe, also have cameras at the head of the robot and they can incline their head [9, 10].

We have developed a pipe inspection robot that uses a spherical ultrasonic motor (SUSM) [11] as the camera actuator and whose aim is to inspect a pipe with an inner diameter of 50 mm. The robot has three rotational DOFs and a compact position sensing system that can be inserted inside the pipe. Since the robot is able to point a camera at any direction, it can directly observe flaws and corrosion; this enables us to accurately determine a flaw's size and condition. Fig. 1 shows a schematic diagram of the pipe inspection robot. The left side of the robot includes an SUSM as the camera actuator and a three-dimensional sensing system using rotary potentiometers. The right side includes the driving circuit for the SUSM and a processing circuit for the sensing system. A spring connects two pods to move in bending pipes. There are several advantages of applying the SUSM to a pipe inspection robot: (1) the motor exhibits a high output torque at low speeds and high responsiveness, (2) the robot, which does not have a reduction gear, has a compact design and simple structure (3) SUSMs have holding torques for braking if the electricity is turned off, (4) the round shape of the SUSM allows the robot to move forward in a curve pipe or joint. However, previous SUSMs, which use a rotating spherical rotor, have the disadvantage that its range of movement is too narrow. In this study, we present a new kind of SUSM, which rotates the outer case with camera, in order to solve the problem of range and to determine the control strategy with a sensing system using potentiometers. The SUSM succeeded in expanding the range of movement and controlling the precisely desired direction.

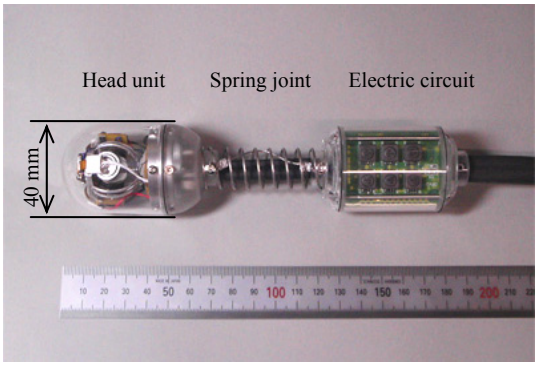

Fig. 1 Schematic diagram of the pipe inspection robot; the left side includes a camera actuator and position sensor, and the right side includes a driving circuit for the actuator and processing circuit for sensors.

This work was supported in part by Japan Science and Technology Agency 1910.

M. Hoshina, and S. Toyama are with Department of Mechanical Systems Engineering Department, Tokyo University of Agriculture and Technology, 2-24-16 Naka-cho, Koganei-city, Tokyo 184-8588 Japan. 50008643230@st.tuat.ac.jp, toyama@cc.tuat.ac.jp. T. Mashimo is with the Robotics Institute, Carnegie Mellon University, 5000 Forbes Avenue, Pittsburgh, PA 15213, USA. tmashimo@cs.cmu.edu

II. Kinematic Design of Actuator and Sensing System

A. Spherical ultrasonic motor

The SUSM comprises three ring-shaped vibrators and one sphere. The vibrator consists of an annular metallic elastic body to which piezoelectric elements are glued. When an AC voltage is applied to the piezoelectric elements, a standing wave is generated on the elastic body. When two AC voltages with a time phase difference are applied to the positive and negative sections of the piezoelectric elements, a traveling-wave is generated due to combination of the two standing-waves [12]. The vibrators provide vibration energy to the sphere by an elliptical motion generated by the traveling wave. We can control the magnitude and direction of the torque by changing the phase difference.

The relationship between the torque T and phase difference ρ in a single vibrator is approximated by the following equation.

$$T = A\sin\rho \tag{1}$$

where A is the maximum value of the torque. The torque of the SUSM is determined by the resultant vector of the vibrators. Fig. 2 (a) and (b) show the locations of the vibrators and sphere along the X-Y and X-Z planes, respectively. The components of the resultant vector generated by each vibrator, $\mathbf{S}_1$, $\mathbf{S}_2$ and $\mathbf{S}_3$, are described by the following equations:

$$\begin{aligned}
\mathbf{S}_1 &= T_1\left[\cos\frac{3}{2}\pi\cos\phi \quad \sin\frac{3}{2}\pi\cos\phi \quad \sin\phi\right]^T \\
\mathbf{S}_2 &= T_2\left[\cos\frac{5}{6}\pi\cos\phi \quad \sin\frac{5}{6}\pi\cos\phi \quad \sin\phi\right]^T \\
\mathbf{S}_3 &= T_3\left[\cos\frac{1}{6}\pi\cos\phi \quad \sin\frac{1}{6}\pi\cos\phi \quad \sin\phi\right]^T
\end{aligned} \tag{2}$$

where T_1, T_2, and T_3 are the scalars of the torque generated by each vibrator, respectively. ϕ is the angle with the X-Y plane, as shown in Fig. 2 (b). The resultant vector of the torque generated by SUSM, $\mathbf{S}$, is described as follows:

$$\mathbf{S} = \mathbf{S}_1 + \mathbf{S}_2 + \mathbf{S}_3 \tag{3}$$

$$\mathbf{S} = \begin{bmatrix} S_x \\ S_y \\ S_z \end{bmatrix} = \begin{bmatrix} \left(-\frac{\sqrt{3}}{2}T_2 + \frac{\sqrt{3}}{2}T_3\right)\cos\phi \\ \left(-T_1 + \frac{1}{2}T_2 + \frac{1}{2}T_3\right)\cos\phi \\ \left(T_1 + T_2 + T_3\right)\sin\phi \end{bmatrix} \tag{4}$$

Here, the torque of the SUSM has three rotational DOFs. By controlling the torque of each vibrator, the SUSM generates a torque between the outer case and the sphere.

B. Definition of rotational direction of SUSM

The rotational direction of the SUSM is defined by the differences in the input phase of each vibrator. To avoid rotating camera footage, the rotation around the Z-axis is restricted when the SUSM is used as a camera actuator in the pipe inspection robot.

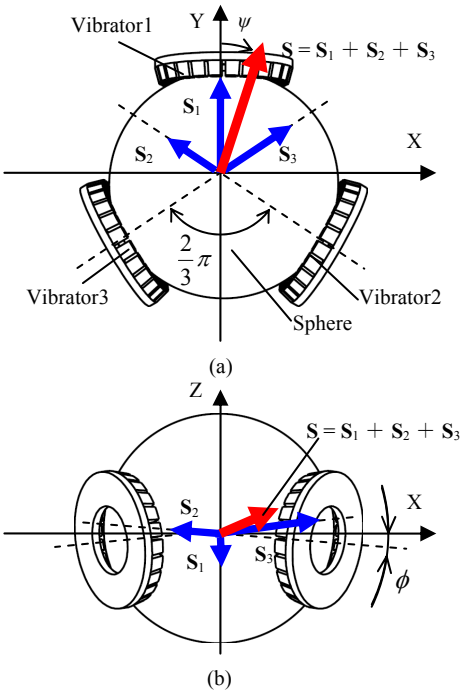

Fig. 2 Location of the vibrators (a) x-y plane, (b) x-z plane.

$$S_z = 0 \tag{5}$$

In addition, the scalar of the SUSM torque should be constant in order to equalize the rotational speeds in all rotational directions.

$$|\mathbf{S}| = B \tag{6}$$

Here, B is a constant number. We defined the angle from the Y-axis, ψ, to the rotational vector on the X-Y plane, as shown in Fig. 2 (a). The torques of each vibrator, T_1, T_2, and T_3, are described by the following equations, Eqs. (4)–(6), respectively:

$$\begin{aligned}
T_1 &= C\cos\psi \\
T_2 &= C\cos\left(\psi + \frac{2}{3}\pi\right) \\
T_3 &= C\cos\left(\psi - \frac{2}{3}\pi\right)
\end{aligned} \tag{7}$$

$$C = \frac{2}{3}\frac{B}{\cos\phi} \tag{8}$$

The torque of the SUSM becomes maximum when the following condition is applied to Eqs. (1) and (7).

$$C_{\max} = A \tag{9}$$

Using Eqs. (6), (8), and (9), the maximum torque of the SUSM is described as follows:

$$|\mathbf{S}|_{\max} = \frac{2}{3}\cos\phi\cdot A \tag{10}$$

The maximum torque of the SUSM is approximately 1.5 times larger than that of one vibrator when the angle ϕ is small. When the rotational direction is given, the input phase

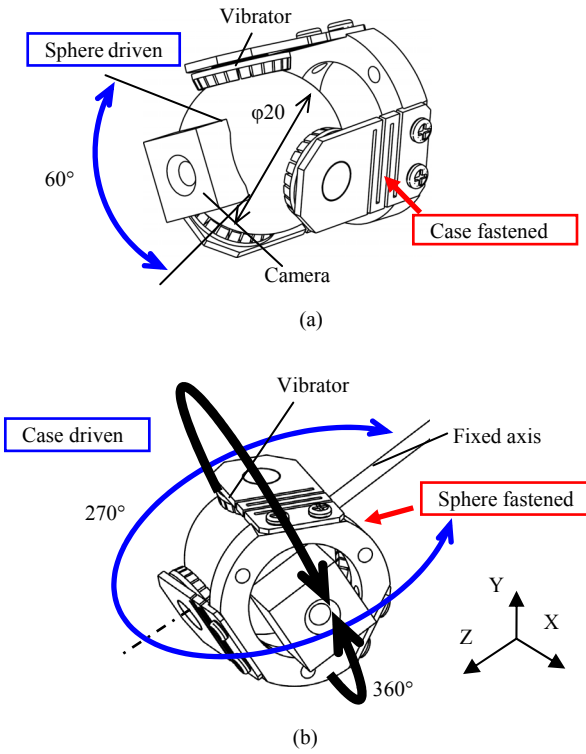

Fig. 3 Differences in the range of movement: (a) Conventional type SUSM, (b) Outer rotor-type SUSM.

differences of each vibrator, ρ_1, ρ_2, and ρ_3, are defined by the following equations:

$$\rho_1 = \sin^{-1}(\cos\psi)$$
$$\rho_2 = \sin^{-1}\left(\cos\left(\psi + \frac{2}{3}\pi\right)\right) \quad (11)$$
$$\rho_3 = \sin^{-1}\left(\cos\left(\psi - \frac{2}{3}\pi\right)\right)$$

C. *Outer rotor-type SUSM*

The camera actuator for the pipe inspection robot requires compactness and a wide range of movement. The range of movement of a conventional SUSM [13, 14] is confined to a range of approximately 60° due to the interference between the camera and vibrator, as shown in Fig. 3 (a). As a result, it cannot fulfill a wide range of motion. To solve this problem, we developed an outer rotor-type SUSM (OR-SUSM). As shown in Fig. 3, the conventional SUSM employs a fixed case and rotates the sphere. In contrast, the OR-SUSM employs a fixed sphere and rotates the outer case. The primary advantage of the OR-SUSM is its wide range of movement. As shown in Fig. 3 (b), the OR-SUSM can avoid interference between the fixed axis and vibrators using the space between each vibrator, and hence, it has an approximately 270° range of movement around the X- and Y-axes. Accordingly, the mechanism makes it possible for the actuator to gaze around the pipe wall circumferentially when the camera is driven first to 90° around the Y-axis and then 360° around the Z-axis. This characteristic of this motion is appropriate for pipe inspection.

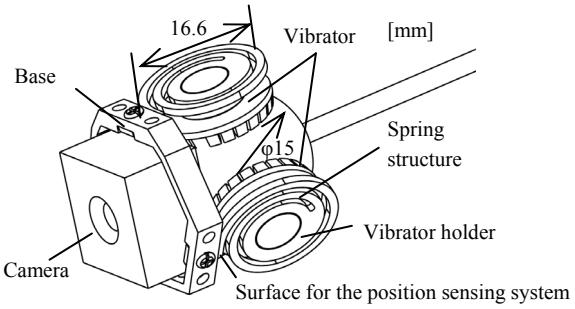

Fig. 4 New case for the outer rotor type.

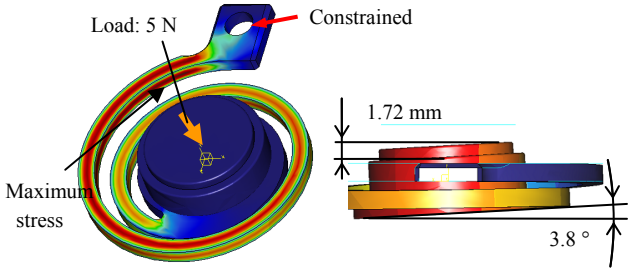

Fig. 5 Results of static analysis by FEM.

The new outer case for a pipe inspection robot, as shown in Fig. 4, was redesigned to miniaturize the robot and reduce the inertia for high performance. Duralumin (AL2011) was used as the base material in place of the stainless material (SUS304), and the excess material was cut. Hence, the mass reduced by roughly 60% from 15.3 g to 6.05 g, and the occupied space reduced by roughly 50% from 12.51 cm^3 to 6.54 cm^3. The occupied space is defined as the product of the top projected area and height. The vibrators must be properly pressed on the sphere, which implies even contact between the vibrator and sphere and a press force of 5 N [15]. The vibrator holder employs a spring structure to prevent uneven contact. The pressing force is determined by the dimensions of the base that is fixing the vibrator holders. Further, it was necessary to decide the vibrator locations and to check whether the vibrators become over-stressed. Therefore, a finite element method (FEM) analysis with a force of 5 N applied on the center of the vibrator holder, and the screw hole constrained was run. Fig. 5 shows the results of static analysis obtained by FEM. The maximum stress is 477 N/mm^2. This value is smaller than the spring deflection limit of 590 N/mm^2. The central part slopes away at 3.8°, and it is displaced by 1.72 mm. By using these values, a new case was designed. Although the case does not have an adjusting mechanism for the compactness, the spring structures of the vibrator holders compensate the error.

D. *Sensing system using rotary potentiometers*

The SUSM requires a position sensor to move to an arbitrary position or to return to the default position. The position sensor should have a small size and should not

reduce the range of movement. Moreover, it must be able to sense three rotational DOFs. Consequently, we developed a position sensing unit consisting of three rotary potentiometers (RDC50), which is manufactured by Alps Electric, and three guides, as shown in Fig. 6. The potentiometers A and B are located 120° to each other and measure the angle using the circular arch-shaped guides A and B. The other potentiometer C is installed on the fixed axis. The clearances of the guides are 0.1 mm. The total size of the SUSM with the sensing unit is smaller than the sphere having a diameter of 45 mm. The accuracy of the sensing unit is 1° because of the clearances of the guides and low rigidity of the guides. The default position is defined as the position when the output axis is coincident with the Z-axis. The default position is located on the line passing through the center of rotation and the intersection of the two circular arch-shaped guides. Therefore, the position vector of the SUSM **D** is described by the cross product of the two unit vectors $\mathbf{R}_\alpha, \mathbf{R}_\beta$ normal to each circle of the guides A and B. We define the rotational angles of potentiometers A, B and C as α, β, and γ, respectively. $\mathbf{R}_\alpha$ and $\mathbf{R}_\beta$ are given as follows:

$$\mathbf{R}_\alpha = \begin{bmatrix} \cos\alpha\cos\frac{1}{3}\pi & -\cos\alpha\sin\frac{1}{3}\pi & -\sin\alpha \end{bmatrix}^T \quad (12)$$

$$\mathbf{R}_\beta = \begin{bmatrix} \cos\beta\cos\frac{1}{3}\pi & \cos\beta\sin\frac{1}{3}\pi & -\sin\beta \end{bmatrix}^T \quad (13)$$

The position vector $\mathbf{D}$ is given as follows:

$$\mathbf{D} = \frac{\mathbf{R}_\alpha \times \mathbf{R}_\beta}{\left|\mathbf{R}_\alpha \times \mathbf{R}_\beta\right|} = \frac{1}{\left|\mathbf{R}_\alpha \times \mathbf{R}_\beta\right|} \begin{bmatrix} \frac{\sqrt{3}}{2}(\cos\alpha\sin\beta + \sin\alpha\cos\beta) \\ \frac{1}{2}(\cos\alpha\sin\beta - \sin\alpha\cos\beta) \\ \frac{\sqrt{3}}{2}\cos\alpha\cos\beta \end{bmatrix} \quad (14)$$

The angle around the Z-axis is measured by potentiometer C. Fig. 7 shows the head of the pipe inspection robot without its cover; its system includes a camera, SUSM, LED, and potentiometers.

III. Experiments on OR-SUSM

A. Evaluation of OR-SUSM

The characteristics of the torque and rotational speed and those of the phase difference and rotational speed were measured. Fig. 8 shows the schematic of the experimental setup. The equipment comprises an SUSM at the center and two rotary encoders (MES-20-3600P) manufactured by MTL located at right angles to each other. The encoders with circular arch-shaped guides measure the rotational angle of the SUSM.

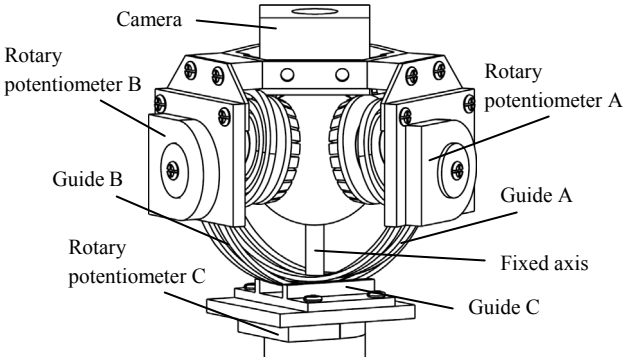

Fig. 6 Position sensing system using rotary potentiometers.

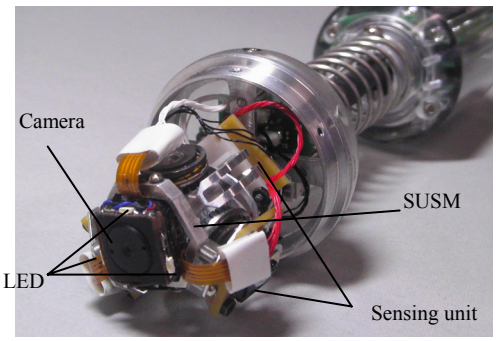

Fig. 7 Head unit of pipe inspection robot with a camera unit in the head of the robot.

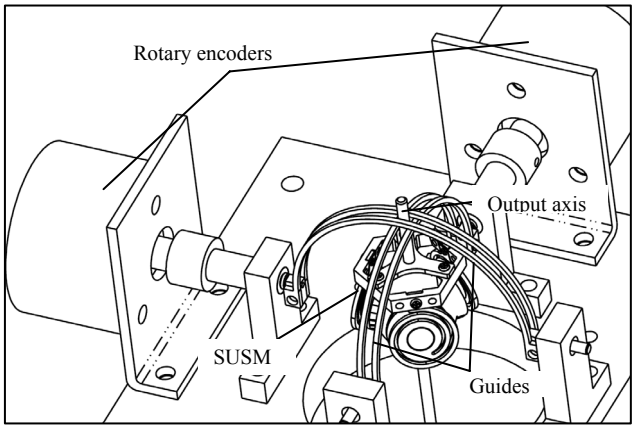

Fig. 8 Schematic of the experimental setup for measuring angle.

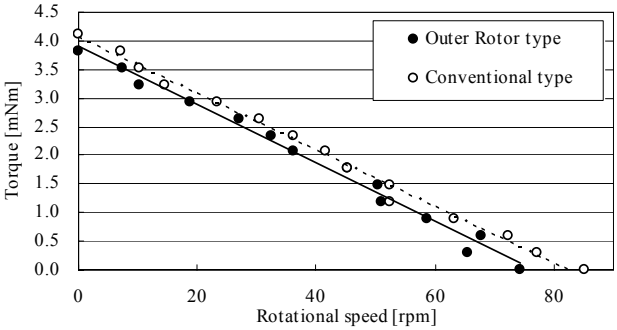

Fig. 9 Relationship between torque and rotational speed.

The relationship between the torque and the rotational speed was measured. The output axis was an added weight with a thread. The amount of weight was varied, and the rotational speed was measured. The rotational speed was measured with a steady speed in order to avoid the effect of the acceleration of the weight. This experiment was conducted with both conventional SUSMs and OR-SUSMs. Fig. 9 shows the results of the characteristics of the torque and rotational speed, indicating that it is linear. There is little difference between the conventional and outer rotor types. The new case has satisfactorily prevented the loss of torque.

The relationship between the phase difference and the rotational speed was measured. When the phase difference of each vibrator is $-\rho_1 = \rho_2 = \rho_3$, the rotational vector of the SUSM, **S**, is described as follows from Eqs. (1) and (4).

$$\mathbf{S} = \begin{bmatrix} 0 \\ 2A \sin \rho_1 \cos \phi \\ A \sin \rho_1 \sin \phi \end{bmatrix} \tag{15}$$

Since the angle to the X-Y plane, ϕ, is very small, $\sin\phi = 0$. The SUSM rotates only around the Y-axis. We varied the phase difference ρ from 90° to –90° in steps of 6° and measured the rotational speed. Fig. 10 shows the relationship between the phase difference and rotational speed. It was confirmed that the rotational speed changes in a sinusoidal manner with the phase difference, as given in Eq. (1). Further, discordance, which is due to the displacement of the position of the piezoelectric elements, existed.

B. Rotational direction control using phase differences

The rotational direction of the SUSM was decided by the phase differences of each vibrator, as shown in Eqs. (11). The SUSM was driven in 12 directions, displaced by 30°, in order to confirm that the SUSM is driven in the designated directions. The angle from the Y-axis to the rotational trajectory of the SUSM on the X-Y plane is defined by ψ', as shown in Fig. 11. Since the rotational trajectory is perpendicular to the rotational vector, ψ' is described as follows:

$$\psi' = \psi + \frac{\pi}{2} \tag{16}$$

Table I shows the input of the phase differences. We measured the trajectories of the output axis with the equipment, as shown in Fig. 8. The SUSM was driven in the designated direction, as shown in Fig. 11, although there are angle errors. The cause of the errors is the individual differences in each vibrator.

C. Hybrid control of frequencies and phase differences

When only the phase differences control is used, there are dead bands and no linearity at low speeds, as shown in Fig. 10. To complement the weakness, the characteristic that rotational speed changes with the frequency of the input voltage can be useful. We propose a new hybrid control

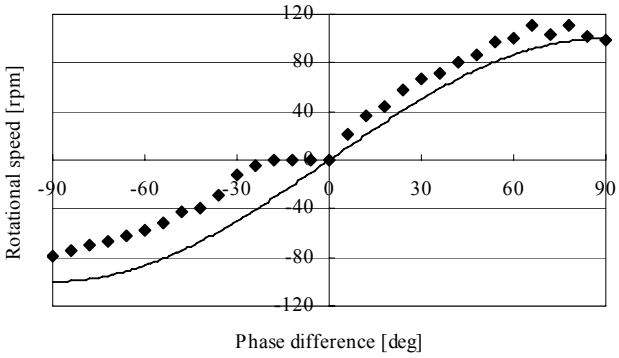

Fig. 10 Relationship between phase difference and rotational speed.

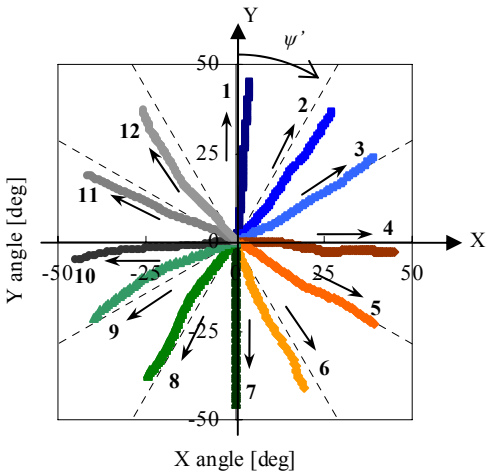

Fig. 11 Output trajectories of the output axis; experimental arrangement.

TABLE I
INPUT VALUE OF PHASE DIFFERENCES FOR EACH DIRECTION

Direction	ψ'	Vibrator1	Vibrator2	Vibrator3
1	0 °	0 °	60 °	-60 °
2	30 °	30 °	90 °	-30 °
3	60 °	60 °	60 °	0 °
4	90 °	90 °	30 °	30 °
5	120 °	60 °	0 °	60 °
6	150 °	30 °	-30 °	90 °
7	180 °	0 °	-60 °	60 °
8	-150 °	-30 °	-90 °	30 °
9	-120 °	-60 °	-60 °	0 °
10	-90 °	-90 °	-30 °	-30 °
11	-60 °	-60 °	0 °	-60 °
12	-30 °	-30 °	30 °	-90 °

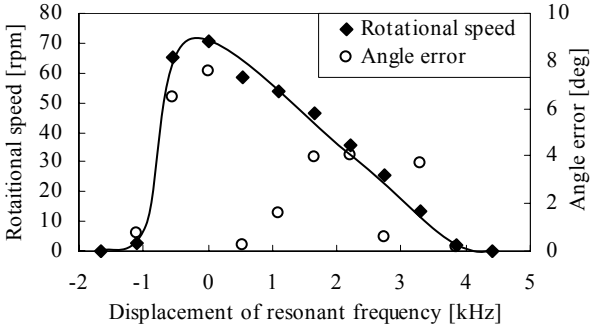

Fig. 12 Relationship between frequency and rotational speed.

method using phase differences for directional control and frequencies for speed control.

The input phase differences are obtained from Eqs. (11). The input frequencies are similarly varied with the resonance frequencies of each vibrator without varying the phase differences. The torque of the SUSM is varied with the ratio of the torques of each vibrator. In this manner, the rotational speed can be varied without varying the rotational direction. In the experiments for evaluating this control method, the phase differences in direction 1, as given in Table I, were inputted. We varied the input frequencies in steps of 0.55 kHz from the resonance frequencies, and we measured the rotational speed and angle error from the desired angle. Fig. 12 shows the results, which indicate that the rotational speed decreased gradually as the input frequencies increased from the resonance frequencies. In addition, the angle error did not increase at low speed. Consequently, this hybrid control method of frequencies and phase differences was effective.

D. Return to default position using hybrid control

The experiment to evaluate the accuracy of return to the default position from 8 directions displaced by 45° was conducted using the sensing system of rotary potentiometers and the hybrid control method. The rotational speed was changed in proportion to the distance from the current position to default position. We evaluated the accuracy of its return to the default position using two rotary encoders in Fig. 8. The SUSM returned to the default position within an accuracy of 1°, as shown in Fig. 13. The accuracy of 1° is the limit of the sensing unit. The SUSM has higher potential. The error of the view is smaller than 1% because the view angle of the camera is 120°. This is sufficient for pipe inspection.

IV. Conclusion

In this study, we developed a novel SUSM (outer rotor-type SUSM) as the camera actuator for a pipe inspection robot. The OR-SUSM dramatically succeeded in expanding the range of movement from 60° to 270°, and decreasing the weight of the case for the OR-SUSM. An FEM analysis and an experiment to evaluate the OR-SUSM were conducted. We have presented a hybrid control strategy using the phase differences and frequencies of applied voltages to move to designated directions. A compact position sensing system using rotary potentiometers was developed. The total size of the pipe inspection robot can be inserted into the interior of a 50-mm inner diameter pipe. By using this sensing system, the SUSM can return to the default position within an accuracy of 1°.

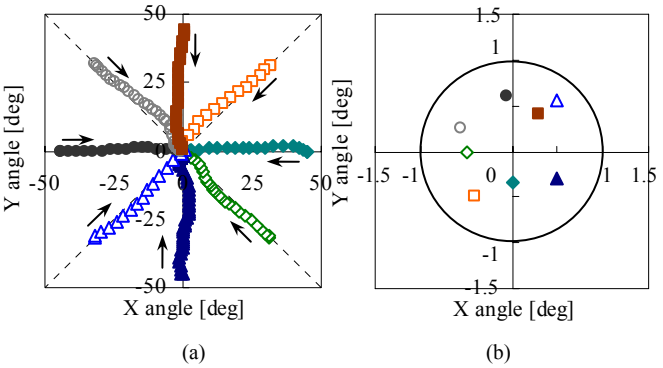

Fig. 13 Accuracy of the zero-point return, (a) Trajectory, (b) Neighborhood of zero-point.

References

[1] T. Fukuda, H. Hosokai, and M. Uemura, "Rubber gas actuator driven by hydrogen storage alloy for in-pipe inspection mobile robot with flexible structure," in *Proceedings of the IEEE International Conference on Robotics and Automation (ICRA1989),*, 1989, pp. 1847-1852

[2] C. Anthierens, A. Ciftci, and M. Betemps, "Design of an electro pneumatic micro robot for in-pipe inspection," in *Proceedings of the IEEE International Symposium on Industrial Electronics (ISIE '99)* 1999, pp. 968-972 vol.2.

[3] C. Chang-Hwan, J. Seung-Ho, and K. Seung-Ho, "Feeder Pipe Inspection Robot Using an Inch-Worm Mechanism with Pneumatic Actuators," in *Proceedings of the IEEE International Conference on Robotics and Biomimetics (ROBIO 2004)*, 2004, pp. 889-894.

[4] A. Brunete, M. Hernando, and E. Gambao, "Modular Multiconfigurable Architecture for Low Diameter Pipe Inspection Microrobots," in *Proceedings of the IEEE International Conference on Robotics and Automation (ICRA 2005)* 2005, pp. 490-495.

[5] T. Matsuoka, H. Okamoto, M. Asano, S. Mitsuishi, and T. Matsui, "A prototype model of micro mobile machine with piezoelectric driving force actuator," in *Proceedings of 5th International Symposium on Micro Machine and Human Science* 1994, p. 47.

[6] T. Idogaki, H. Kanayama, N. Ohya, H. Suzuki, and T. Hattori, "Characteristics of piezoelectric locomotive mechanism for an in-pipe micro inspection machine," in *Proceedings of the Sixth International Symposium on Micro Machine and Human Science (MHS '95)* 1995, pp. 193-198.

[7] T. Fukuda, H. Hosokai, H. Ohyama, H. Hashimoto, and F. Arai, "Giant magnetostrictive alloy (GMA) applications to micro mobile robot as a micro actuator without power supply cables," in *Proceedings of An Investigation of Micro Structures, Sensors, Actuators, Machines and Robots. Micro Electro Mechanical Systems (MEMS '91),* , 1991, pp. 210-215.

[8] K. Suzumori, T. Miyagawa, M. Kimura, and Y. Hasegawa, "Micro inspection robot for 1-in pipes," *IEEE/ASME Transactions on Mechatronics,* vol. 4, no. 3, pp. 286-292, 1999.

[9] S. Hirose, *Biologically Inspired Robots: Snake-like Locomotors and Manipulators*: Oxford University Press, 1993.

[10] S. Wakimoto, J. Nakajima, M. Takata, T. Kanda, and K. Suzumori, "A micro snake-like robot for small pipe inspection," in *Proceedings of 2003 International Symposium on Micromechatronics and Human Science (MHS 2003)*, 2003, pp. 303-308.

[11] S. Toyama, S. Sugitani, G. Zhang, Y. Miyatani, and K. Nakamura, "Multi degree of freedom spherical ultrasonic motor," in *Proceedings. IEEE International Conference on Robotics and Automation (ICRA1995)* 1995, pp. 2935-2940 vol.3.

[12] T. Sashida and T. Kenjo, *An introduction to ultrasonic motors*. Oxford, U.K: Clarendon, 1993.

[13] E. Purwanto and S. Toyama, "Control method of a spherical ultrasonic motor," in *Proceedings of IEEE/ASME International Conference on Advanced Intelligent Mechatronics (AIM 2003)* 2003, pp. 1321-1326 vol.2.

[14] T. Mashimo, K. Awaga, and S. Toyama, "Development of a Spherical Ultrasonic Motor with an Attitude Sensing System using Optical Fibers," in *Proceedings of the IEEE International Conference on Robotics and Automation (ICRA2007)*, 2007, pp. 4466-4471.

[15] T. Mashimo, S. Toyama, and H. Ishida, "Development of an MRI Compatible Surgical Assist Manipulator using Spherical Ultrasonic Motor (1st report)-Prototype of the Spherical Ultrasonic Motor-," *Journal of the Japan Society for Precision Engineering* vol. 73, no. 2, pp. 275-280, 2007 (in Japanese).